

Modelling of an optimized BLDC motor energized by a sinusoidal voltage source

Abstract. The article proposes the optimization of BLDC motor control by using the load-dependent leading phase with respect to the rotor angular position, which determines the waveform of the sinusoidal voltage supplying the motor. Such strategy results in faster motor's time responses compared to the motor without control optimization. In addition, by using a sinusoidal voltage source to energize the BLDC motor, the distortions of both the phase currents and the motor torque, visible in the form of ripples, were reduced.

Streszczenie. W artykule zaproponowano optymalizację sterowania silnikiem BLDC poprzez wykorzystanie zależnego od obciążenia wyprzedzenia fazowego względem położenia kąтового wirnika, które określa przebieg sinusoidalnego napięcia zasilającego silnik. Taka strategia skutkuje szybszymi odpowiedziami czasowymi silnika w porównaniu z silnikiem bez optymalizacji sterowania. Dodatkowo poprzez zastosowanie źródła napięcia sinusoidalnego do zasilania silnika BLDC zredukowano zniekształcenia zarówno prądów fazowych, jak i momentu silnika, widoczne w postaci tętnień. (Modelowanie optymalizowanego silnika BLDC zasilanego z sinusoidalnego źródła napięcia).

Keywords: BLDC motor, control strategies and optimization, sinusoidal and trapezoidal control, mathematical modelling.

Słowa kluczowe: silnik BLDC, strategie i optymalizacja sterowania, sterowanie sinusoidalne i trapezoidalne, modelowanie matematyczne.

Introduction

Brushless DC (BLDC) motors [1–4] together with permanent magnet synchronous motors (PMSM) [5–9] belong to the group of permanent magnet motors (PMM). There are two types of PMM: motors with a trapezoidal induced voltage (applies mainly to BLDC motors) and motors with a sinusoidal induced voltage (applies mainly to PMSM). This division results from different ways of connecting the coils in the stator winding and different ways of forming the magnetic field distribution in the motor air-gap by appropriate magnetization of permanent magnets or shaping the rotor pole shoes. Motors with sinusoidal induced voltage are characterized by sinusoidal currents and smooth torque, in contrast to the distorted currents and the rippling torque of the motor with a trapezoidal induced voltage, causing additional vibrations and noise.

The brushless DC motor is a combination of a permanent magnet synchronous motor and an electronic commutator (inverter). It is possible to activate semiconductor switches (transistors) of the inverter supplying the synchronous motor from an independent voltage-controlled pulse generator or from an angular position transducer coupled with the motor shaft. In the latter case, the effect of switching the stator phase windings in specific rotor positions is analogous to the operation of a mechanical commutator in a brushed DC motor. The properties of the synchronous motor controlled in this way are then similar to those of a separately excited DC motor.

In order to determine the angular position of a BLDC motor shaft, Hall sensors mounted in the stator are most often used. These sensors together with permanent magnets mounted on the rotor form a magnetic encoder. Instead of a magnetic encoder, optical encoders or rotary electrical transformers, two-phase (resolver) or three-phase (synchro), can be used to measure the angular position of the rotor [1,2]. Contrary to the most popular optical encoders, rotary electrical transformers are resistant to vibration, shock, dust and moisture, and to long-term operation at high temperatures. Their disadvantage is the lower accuracy of the measurement. The rotor of the rotary electrical transformer is excited with alternating current of a carrier frequency at least ten times higher than the frequency corresponding to the maximum speed of the motor. The magnetic field produced by the rotor current

induces back electromotive forces in the stator phase windings of the rotary electrical transformer.

In BLDC motor control, the pulse width modulation (PWM) method is frequently used to limit the starting current as well as to control the speed and torque of the motor.

Modelling of the BLDC motor

The paper [1] proposes a mathematical model of a three-phase BLDC motor and presents the results of computer simulation and experimental verification. The comparison of these results shows a high level of adequacy of the proposed model. This model is based on the equivalent circuit of an inverter-fed BLDC motor as shown in Fig. 1b. The abovementioned equivalent circuit is universal in terms of its applicability to the formulation of equations describing a BLDC motor energized by both a four-wire line (with a neutral wire) and a three-wire line, with the resistance value R_0 being 0 or ∞ , respectively. Instead of $R_0 = \infty$, for numerical calculations, a sufficiently large value of the resistance R_0 can be adopted, i.e. several orders of magnitude greater than the rated impedance defined on the basis of the motor's rated phase parameters, i.e. $R_0 \gg U_{n(ph)} / I_{n(ph)}$. The mathematical model of the BLDC motor is presented in [1]:

$$(1) \quad \mathbf{u} = R\mathbf{i} + \dot{\boldsymbol{\psi}} + \mathbf{e}$$

where $\mathbf{u} = [u_a \ u_b \ u_c]^T$, $\mathbf{i} = [i_a \ i_b \ i_c]^T$, $\boldsymbol{\psi} = [\psi_a \ \psi_b \ \psi_c]^T$, $\mathbf{e} = [e_a \ e_b \ e_c]^T$ are vectors of the terminal voltages of the motor phase windings, phase currents, phase flux linkages and back electromotive forces induced in the motor phase windings, respectively,

$$(2) \quad \mathbf{i} = (L - M)^{-1}(\boldsymbol{\psi} + M\mathbf{i}_0)$$

$$(3) \quad i_0 = (L + 2M)^{-1}(\psi_a + \psi_b + \psi_c)$$

where $\mathbf{i}_0 = [i_0 \ i_0 \ i_0]^T$ is the vector of the phase currents' sums, i.e. $i_0 = i_a + i_b + i_c$, L is the phase self-inductance of the motor winding: $L = L_\sigma + L_{ar}$, L_σ is the leakage inductance, L_{ar} is the armature reaction inductance, M is the mutual inductance between the motor phase windings: $M = -L_{ar}/3$ or $-L_{ar}/2$ depending on the design of the motor winding, then $L - M = L_\sigma + 4L_{ar}/3$ or $L_\sigma + 3L_{ar}/2$, respectively.

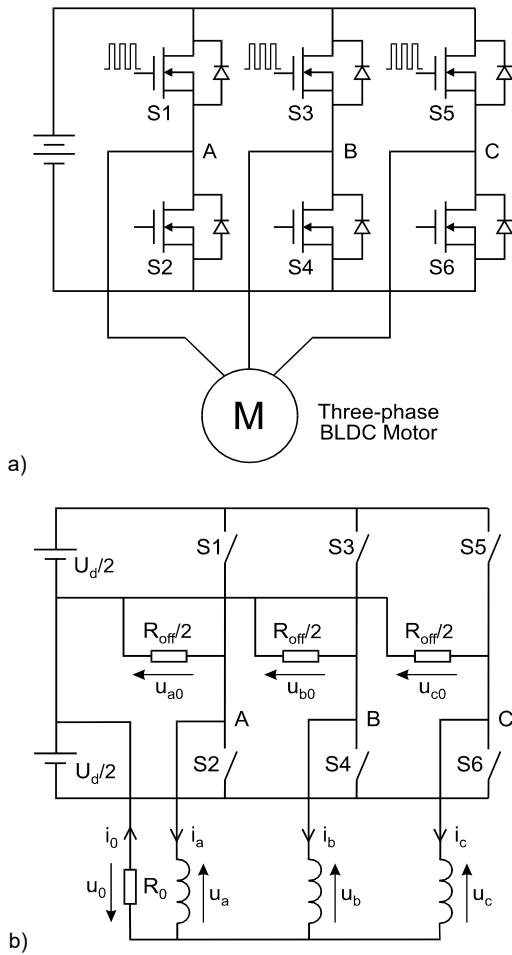


Fig. 1. Three-phase BLDC motor energized by a voltage source inverter controlled by the PWM method (a), and an equivalent circuit of the inverter-fed BLDC motor (b), where $R_0 = \infty$ in the case of a motor energized without neutral conductor

The following relationship can be used to calculate the back electromotive forces:

$$(4) \quad \mathbf{e} = N_p \Psi_p \omega_m \mathbf{f}$$

where $\mathbf{f} = [f_a(\theta_e) \ f_b(\theta_e) \ f_c(\theta_e)]^T$, Ψ_p is the flux linkage excited by the rotor's permanent magnets, ω_m is the angular velocity of the rotor, N_p is the number of pole pairs. The following dependencies can be adopted in order to approximate the functions f_a, f_b, f_c :

$$f_a(\theta_e) = k_f \sin(\theta_e) \quad \cap \quad |f_a(\theta_e)| \leq 1$$

$$f_b(\theta_e) = k_f \sin(\theta_e - 2\pi/3) \quad \cap \quad |f_b(\theta_e)| \leq 1$$

$$f_c(\theta_e) = k_f \sin(\theta_e - 4\pi/3) \quad \cap \quad |f_c(\theta_e)| \leq 1$$

where $k_f = 2$ for the trapezoidal back electromotive force approximation with a wide trapeze base (120 electrical degrees), $\theta_e = N_p \theta_m$, $\theta_e \in [0^\circ; 360^\circ)$, θ_m is the angle of rotor's rotation. The equation of motion of the rotor and the rotating masses attached to it is as follows:

$$(5) \quad \frac{d^2}{dt^2} \theta_m = \frac{d}{dt} \omega_m = J^{-1} (\tau_e - \tau_L)$$

where J is the moment of rotor's inertia, τ_L is the load torque and τ_e is the motor torque:

$$(6) \quad \tau_e = N_p \Psi_p \mathbf{f}^T \mathbf{i}$$

The conventional approach to BLDC motor control is based on the logic states of Hall sensors subjected to the magnetic field of the rotor's permanent magnets. Hall sensors mounted in the stator together with the rotor's permanent magnets form a magnetic encoder which, in the case of a three-phase motor, allows the angular position of the rotor to be measured with an accuracy of 60 electrical degrees. The three-phase BLDC motor control strategy, based on the logic states generated by the magnetic encoder, is presented in [1]. According to the equivalent circuit shown in Fig. 1b, for the selected range of the rotor's angular position $30^\circ < \theta_e \leq 90^\circ$, the following dependencies can be written:

$$(7) \quad u_0 = R_0 i_0, \quad u_a = \frac{1}{2} u_d - u_0, \quad u_b = -\frac{1}{2} u_d - u_0$$

$$u_{c0} = \frac{1}{2} R_{off} i_c \quad \cap \quad -\frac{1}{2} u_d \leq u_{c0} \leq +\frac{1}{2} u_d, \quad u_c = -u_{c0} - u_0$$

where R_{off} is the drain-to-source resistance of the turned off transistor. The dependencies for the successive ranges of the rotor's angular position are similar.

Controlling the BLDC motor with the use of logic states generated by the magnetic encoder enables the motor's phase windings to be energized with voltage of a trapezoidal waveform obtained from a trapezoidal voltage source (TVS). The main disadvantage of such a solution are significant distortions of both the phase currents and the motor torque, visible in the form of ripples. Partial, but a very effective solution to the abovementioned problem is that the BLDC motor is energized by a sinusoidal voltage source (SVS) synchronized directly with the angular position of the rotor:

$$u_a = U_m \sin(\theta_e) - u_0$$

$$(8) \quad u_b = U_m \sin(\theta_e - 2\pi/3) - u_0$$

$$u_c = U_m \sin(\theta_e - 4\pi/3) - u_0$$

However, the work [2] shows the negative impact of using such a source to energize a BLDC motor due to a significant increase in the amplitude of the current and a significant deterioration of dynamics. Therefore, it has been proposed to optimize the BLDC motor control by using the load-dependent leading phase with respect to the rotor angular position, which determines the waveform of the sinusoidal voltage supplying the motor (Fig. 2). At the present stage of research, the motor's supply unit, consisting of a pulse width modulator (PWM), an electro-insulated transistors' driver and a voltage source inverter, has been replaced with an ideal SVS generating a smooth waveform.

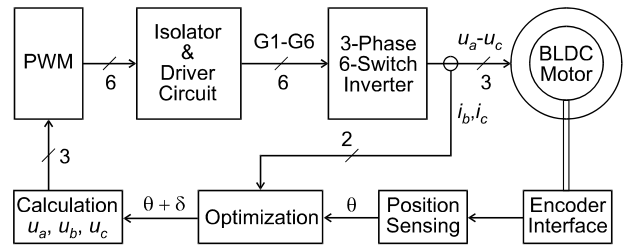


Fig.2. Block diagram of the structure corresponding to the proposed control strategy for the BLDC motor [2]

Contrary to the sometimes used leading commutation of BLDC motor with constant phase angle, in the proposed solution the leading phase angle depends on the motor load, which allows for effective control optimization regardless of changes in this load. The tangent of the abovementioned load-dependent phase angle can be calculated as follows:

$$(9) \quad \tan(\delta) = \frac{2L\tau_e}{3N_p\psi_p^2}$$

The coefficient of 2/3 in the above equation results from the transformation of the three-phase motor equations to the Cartesian coordinate system. A slight reduction of the value of this coefficient, e.g. to 1/2, improves the stability of the control system. The values of the delta angle in equation (9), corresponding to the real motor loads, are usually in the range of $\pm\pi/12$ rad, for which an approximate relationship can be written:

$$(10) \quad \delta \approx \sin(\delta) \approx \tan(\delta) \Leftrightarrow |\delta| \leq \frac{\pi}{12} \text{ rad}$$

Finally, the optimization of the motor control is achieved by introducing the delta angle as the leading phase to the supply voltages (first components in the following phase voltages):

$$(11) \quad \begin{aligned} u_a &= U_m \sin(\theta_e + \delta) - u_0 \\ u_b &= U_m \sin(\theta_e + \delta - 2\pi/3) - u_0 \\ u_c &= U_m \sin(\theta_e + \delta - 4\pi/3) - u_0 \end{aligned}$$

wherein during the motor start-up, the amplitude of the supply voltage U_m was changed according to the time ramp until the set level was reached.

Computer simulation results

The following rated parameters of the BLDC motor were taken into account in the simulation tests: 4 kW, 400 V, 1500 rpm, 11.5 A, 0.025 kgm², $R_s = 0.5$ Ohm, $L_{ar} = 7.4$ mH, $L_{\sigma} = 1.6$ mH, $N_p\omega_h\psi_p = 170$ V.

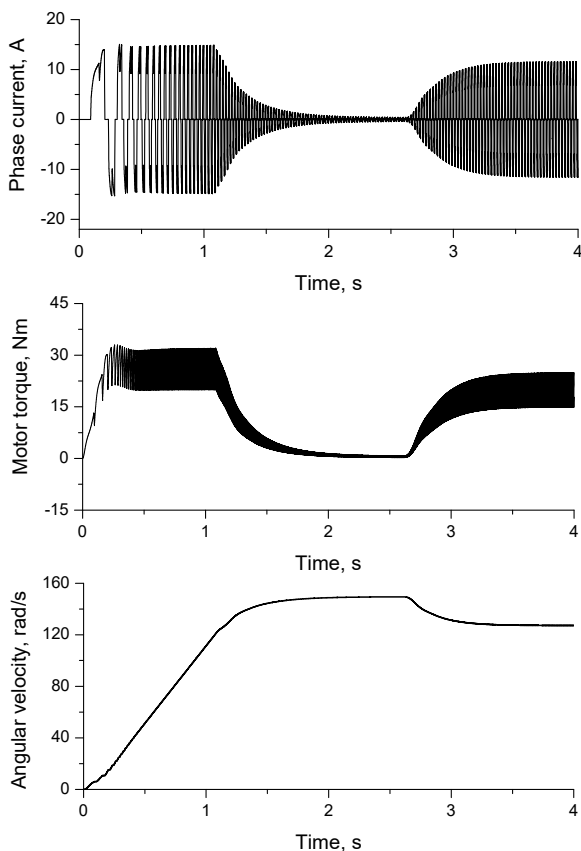


Fig. 3. Phase current, torque and angular velocity of the BLDC motor energized by the TVS during start-up and operation under load

In the simulation tests performed, the motor was connected to a set of rotating masses, which together with the steel drive shaft formed a dual-mass system [4,5,10]. The motor was loaded with the rated braking torque via the above-mentioned working mechanism. Fig. 3 shows the time dependencies of the BLDC motor energized by the TVS during start-up and during operation under rated load, while Figs. 4 and 5 show the time dependencies of the BLDC motor under load in a limited time range.

As mentioned in the previous section, controlling the BLDC motor using the logic states generated by the magnetic encoder enables the motor's phase windings to be energized with a trapezoidal voltage. The main disadvantage of this solution is the significant deformation of both the phase currents and the motor torque, visible in the form of ripples, as shown in Figure 4.

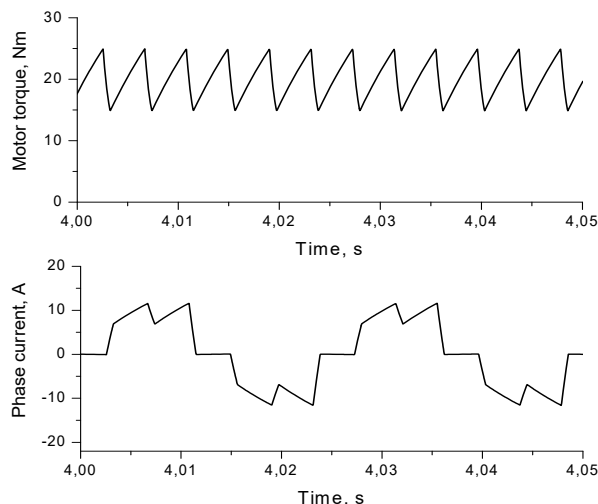


Fig. 4. The torque and phase current of the loaded BLDC motor energized by the TVS

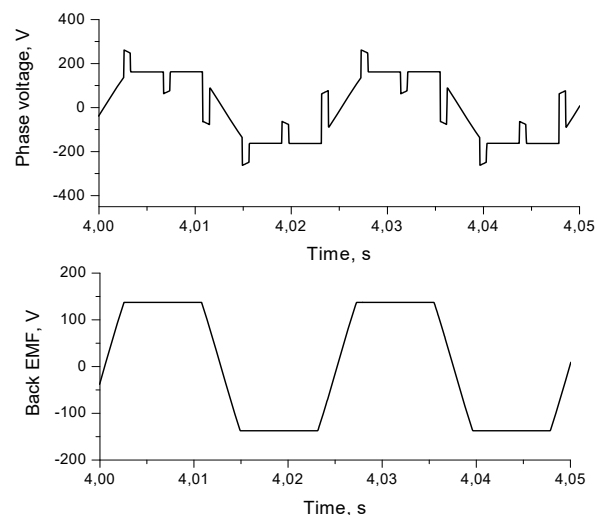


Fig. 5. Phase voltage and induced voltage of the loaded BLDC motor energized by the TVS

A partial, but very effective solution to the abovementioned problem is to energize the BLDC motor by the SVS generating a waveform depending on the angular position of the rotor in accordance with equations (8). Fig. 6 shows the time dependencies of the BLDC motor energized by the SVS during start-up and during operation under rated load, while Figs. 7 and 8 show the time dependencies of the BLDC motor under load in a limited time range.

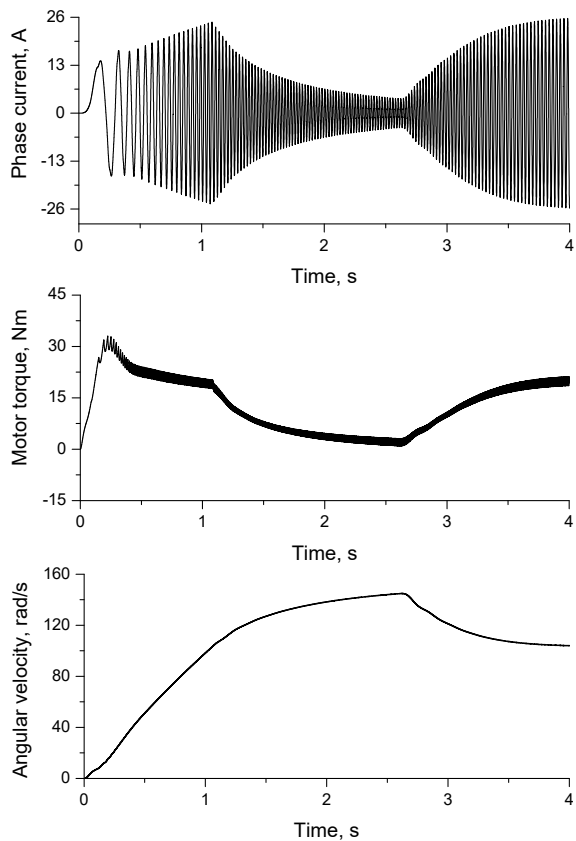


Fig. 6. Phase current, torque and angular velocity of the BLDC motor energized by the SVS during start-up and operation under load

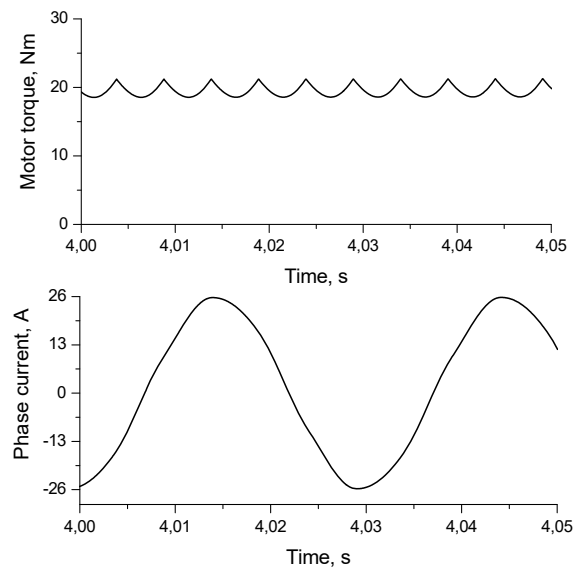


Fig. 7. The torque and phase current of the loaded BLDC motor energized by the SVS

The use of SVS to energize the BLDC motor significantly reduced the amplitude of the motor torque ripple (see the upper graphs in Fig. 4 and 7), and the phase current is practically sinusoidal (lower graph in Fig. 7). Unfortunately, the dynamics of the motor deteriorated significantly and the settling time required for the torque and speed to reach and stay steady state was significantly lengthened (see Fig. 3 and Fig. 6). The amplitude of the phase current also increased significantly (see the lower graphs in Figures 4 and 7).

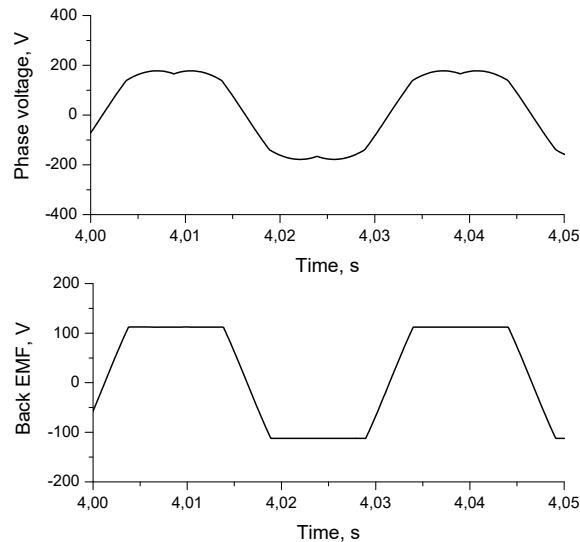


Fig. 8. Phase voltage and induced voltage of the loaded BLDC motor energized by the SVS

The unfavourable phenomena related to the supply of the BLDC motor by the SVS generating a waveform dependent on the angular position of the rotor in accordance with equations (8) can be avoided by using the optimization consisting in controlling the leading phase of this waveform depending on the motor load, as shown in Fig. 2 and equations (9) and (11). Fig. 9 shows the time dependencies of the optimized BLDC motor energized by the SVS during start-up and operation under rated load, while Figs. 10 and 11 show the time dependencies of the BLDC motor under load in a limited time range.

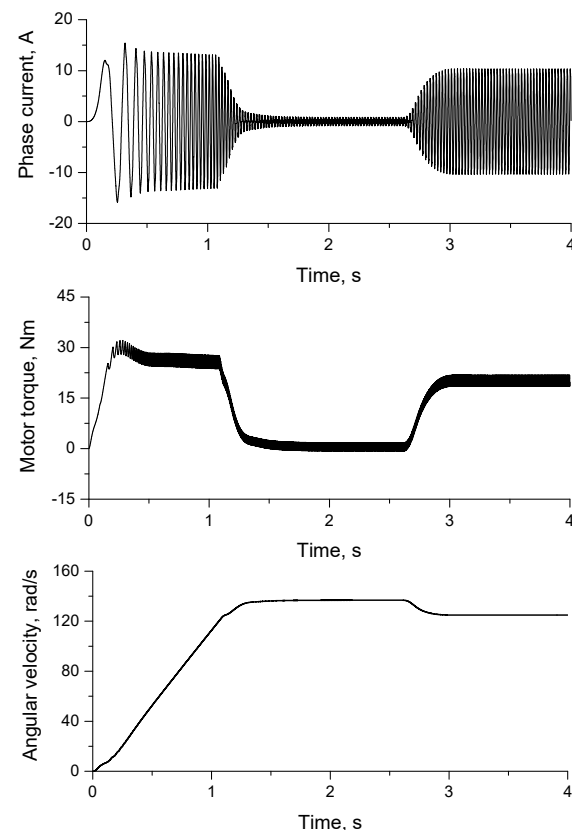


Fig. 9. Phase current, torque and angular velocity of the optimized BLDC motor energized by the SVS during start-up and operation under load

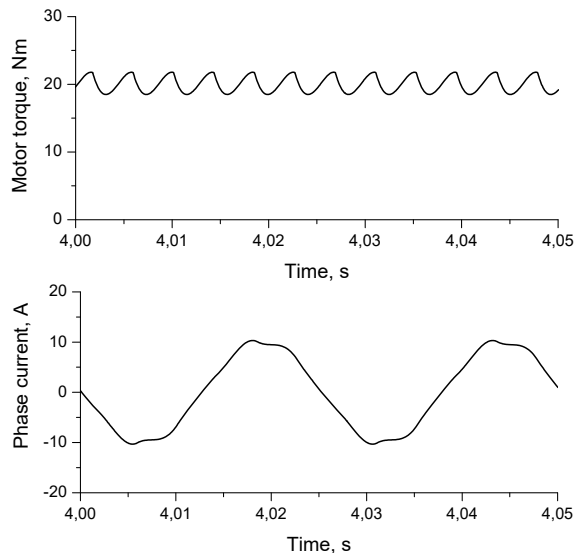


Fig. 10. The torque and phase current of the optimized BLDC motor energized by the SVS during operation under load

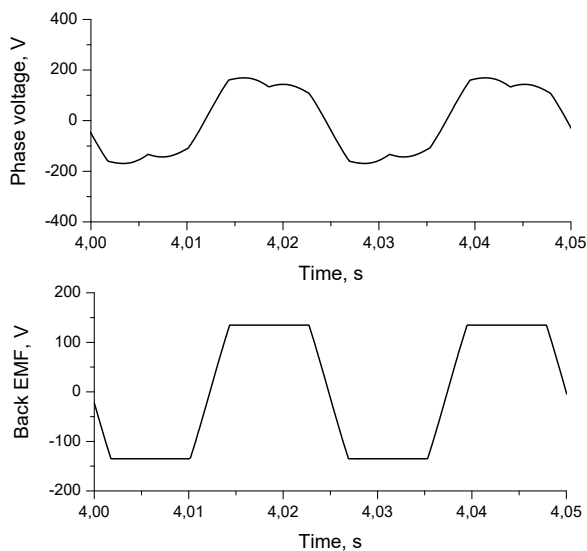


Fig. 11. Phase voltage and induced voltage of the optimized BLDC motor energized by the SVS during operation under load

The use of BLDC motor supply optimization results in the response curves reaching the steady state much faster compared not only to the non-optimized motor energized by the SVS but also to the motor energized by the TVS (see Figures 3, 6 and 9). On the other hand, a slight increase in the amplitude of the torque ripple and a slightly greater distortion of the phase current can be noticed in relation to the non-optimized motor (see Figures 7 and 10). However, in Figures 7 and 8 for a motor without optimization, it is possible to observe that the phase current lags both the phase voltage and the induced voltage (back EMF), while the current of the optimized motor (lower graph in Fig. 10) is in phase with the phase voltage and with the induced voltage (Fig. 11).

Sinusoidal supply of a star-connected three-phase BLDC motor winding without a neutral conductor does not imply sinusoidal phase voltages (see Figures 8 and 11) because the star point potential is not constant and shifts due to balancing the phase currents at this point.

Conclusions

In the article the optimization of BLDC motor sinusoidal supply, based on load-dependent leading phase angle was proposed and the results of computer simulation were presented. Contrary to the sometimes used leading commutation of BLDC motor with constant phase angle, in the proposed solution the leading phase angle depends on the motor load, which allows for effective control optimization regardless of changes in this load. Such optimization results in faster motor's time responses compared to the motor without control optimization. In addition, as a result of the use of the sinusoidal voltage source to energize the BLDC motor, a significant reduction in the ripple of both the phase currents and the motor torque was achieved in relation to the motor energized by the trapezoidal voltage source.

Authors: Andrzej Popenda, PhD, D.Sc., Associate Prof. and Marcjjan Nowak, M.Sc., Czestochowa University of Technology, Faculty of Electrical Engineering, 17 Armii Krajowej av, 42-200 Czestochowa, E-mail: andrzej.popenda@pcz.pl, marcjjan.nowak@pcz.pl

REFERENCES

- [1] Popenda A., Modelling of BLDC motor energized by different converter systems, *Przegląd Elektrotechniczny*, 94 (2018), nr 1, 81-84
- [2] Popenda A., A control strategy of a BLDC motor, *Przegląd Elektrotechniczny*, 89 (2013), nr 12, 188-191
- [3] Shchur I., Lis M., Biletskyi Y., Passivity-Based Control of Water Pumping System Using BLDC Motor Drive Fed by Solar PV Array with Battery Storage System, *Energies*, 14 (2021), no. 8184, 1-25
- [4] Nowak M., Analiza stanów dynamicznych układu napędowego zawierającego silnik BLDC oraz długi element sprężysty, *Przegląd Elektrotechniczny*, 89 (2013), nr 12, 302-305
- [5] Chaban A., Lis M., Szafraniec A., Voltage Stabilisation of a Drive System Including a Power Transformer and Asynchronous and Synchronous Motors of Susceptible Motion Transmission, *Energies*, 15(3) (2022), no. 811, 1-22
- [6] Lis M., Chaban A., Mathematical model of electrical system including transformer and electrical drives based on induction motors and synchronous motors, *E3S Web of Conferences (PE 2018)*, 84 (2019), no. 0200, 1-8
- [7] Szafraniec A., Mathematical model of a drive system with synchronous motors and vertical pumps, *E3S Web of Conferences (PE 2018)*, 84 (2019), 02015, pp. 1-9
- [8] Olesiak K., Application of a Fuzzy Logic Controller for a Permanent Magnet Synchronous Machine Drive, *Przegląd Elektrotechniczny*, 92 (2016), nr 12, 113-116
- [9] Chaban A., Perzyński T., Popenda A., Figura R., Levoniuk V., Mathematical Modeling of Transient Processes in the Susceptible Motion Transmission in a Ship Propulsion System Containing a Shaft Synchronous Generator, *Energies*, 15(9) (2022), no. 3266; 1-17
- [10] Kabziński J., Mosiołek P., Integrated, Multi-Approach, Adaptive Control of Two-Mass Drive with Nonlinear Damping and Stiffness, *Energies*, 14 (2021), no. 5475, 1-24